Communications Earth & Environment

Article in Press

https://doi.org/10.1038/s43247-026-03702-w

Northern permafrost represents a limit on the northward shift of climatically feasible agricultural frontiers under future warming

Received: 7 December 2025

Accepted: 26 May 2026

Cite this article as: Xu, S., Xiao, C., Jägermeyr, J. *et al.* Northern permafrost represents a limit on the northward shift of climatically feasible agricultural frontiers under future warming. *Commun Earth Environ* (2026). https://doi.org/10.1038/s43247-026-03702-w

Song Xu, Cunde Xiao, Jonas Jägermeyr, Vladimir E. Romanovsky, Zhao Zhang, Jianping Duan, Bo Su & Tong Zhang

Northern permafrost represents a limit on the northward shift of climatically feasible agricultural frontiers under future warming

Song Xu[1], Cunde Xiao[1*], Jonas Jägermeyr[2, 3, 4], Vladimir E. Romanovsky[5], Zhao Zhang[6], Jianping Duan[1], Bo Su[1, 7, 8, 9] & Tong Zhang[1]

[1]*State Key Laboratory of Earth Surface Processes and Disaster Risk Reduction, Faculty of Geographical Science, Beijing Normal University, Beijing 100875, China;*

[2]*NASA Goddard Institute for Space Studies, New York, NY, USA;*

[3]*Columbia University, Center for Climate Systems Research, New York, NY, USA;*

[4]*Potsdam Institute for Climate Impacts Research (PIK), Member of the Leibniz Association, Potsdam, Germany;*

[5]*Geophysical Institute, University of Alaska Fairbanks, Fairbanks, AK, USA;*

[6]*Joint International Research Laboratory of Catastrophe Simulation and Systemic Risk Governance, School of National Safety and Emergency Management, Beijing Normal University, Beijing, P. R. China;*

[7]*School of Environment, Beijing Normal University, Beijing 100875, China;*

[8]*Regional Climate Group, Department of Earth Sciences, University of Gothenburg, Gothenburg 40530, Sweden;*

[9]*Stockholm Resilience Centre, Stockholm University, Stockholm 10691, Sweden.*

*e-mail: cdxiao@bnu.edu.cn

Abstract

Global warming is expected to shift crop suitability northward, but the role of permafrost remains unclear. Here we integrate permafrost degradation impacts to project the suitability of seven major crops across the Northern Hemisphere (30°N–83°N). By the end of the century, the northern boundary of crop climatic suitability zones shifts northward by ~331 km and ~739 km under the SSP1–2.6 and SSP5–8.5 scenarios, respectively. Considering this shift and permafrost degradation, zones with persistent near-surface permafrost remain limited (~5%) but vary widely (3–19%) across different permafrost degradation assumptions. By the end of the century, newly emerging frontiers of climatically feasible agriculture reach 4.86 and 11.64 million km² under SSP1–2.6 and SSP5–8.5, respectively, of which 29% and 18% may remain unsuitable for cultivation due to persistent permafrost thaw disturbances. Our results indicate that permafrost is a non-negligible constraint on the northward shift of climatically feasible agricultural frontiers.

Introduction

Climate warming is expected to create new climatically feasible agricultural frontiers (hereafter referred to as AF), particularly in high-latitude and high-altitude regions[1–3]. Against the backdrop of well-documented negative impacts of climate warming on current food systems[4–6], the question whether cold northern regions, currently constrained by harsh climatic conditions, will unlock agricultural potential in the future has increasingly attracted scholarly attention[7]. In some cold-region local communities, several examples have already validated the existence of this potential[8,9].

Climate change has led to global yield reductions of 10% for wheat, 4% for maize, and 13% for barley[10]. Without adaptation, total crop yields in temperate and tropical regions are projected to decline substantially[11]. Under high-end warming scenarios, simulated crop yield losses range from 7% to 23%[12]. In particular, main

crops are expected to be negatively affected in tropical and subtropical regions[13,14]. Worse still, past climate and crop models have underestimated the risk of simultaneous yield failures in current major breadbasket regions[15]. The impacts of climate change on global agriculture may occur earlier than previously anticipated, further narrowing the window for adaptation[16]. Increased frequency and duration of extreme weather events[17] continue to threaten global food security[18]. The demand for agricultural climate adaptation is rising sharply[19,20], however, some climate adaptation measures may negatively affect agricultural markets and food security[21]. Achieving the 1.5 °C target could lead to a 13% reduction in global cropland area[22]. Common adaptation measures may increase soil greenhouse gas emissions[23], and most current croplands face challenges in achieving both emission reduction and yield gains[24]. Therefore, ensuring food security under climate change require substantial investments in technological innovation, cropland expansion, or further adaptation measures[25].

On the other hand, the impacts of climate change on agriculture are not entirely negative. Some scholars suggest that northern agriculture may benefit from climate warming and enhance local food supply[26]. In these cold regions, both crop diversity[19] and yield potential[27] are expected to increase under future warmer climate scenarios. Although such changes may primarily support local-scale food diversification in northern communities, broader climatic suitability projections nevertheless indicate a substantial poleward shift in potential agricultural zones. Globally, according to previous studies, the projected northward shift of the agricultural climatic boundary by the end of this century ranges between 500 and 1,200 km[2,28]. Under the Special Report on Emissions Scenarios (SRES) A1B scenario, climate change would result in an additional 5.6 million km² of land becoming climatically suitable for crop cultivation by the end of the century[1]. Under the RCP 4.5 scenario, agricultural frontiers would cover 8.1–20.0 million km² of the Earth's surface (equivalent to 31–77% of the currently cultivated area) by 2060–2080[3]. Under the RCP4.5 scenario, approximately 1.85 million km² of land in northern Canada would be at least climatically suitable, although it is currently too cold for cultivation. The breadbasket in North America are projected to shift poleward by an average of 600 km by the end of the century under the RCP8.5 scenario[30].

However, the extent of northern agricultural suitability zones remains insufficiently understood[9]. Previous studies have primarily focused on the influence of environmental factors such as climate, soil, and topography on future agricultural suitability in northern regions[2,29,30], yet this poleward shift of suitable areas is also constrained by the presence of permafrost, which is usually not considered in existing studies. Currently, permafrost and its dynamics pose numerous challenges to agricultural cultivation, even under climatically suitable conditions. Farming in Yakutia requires substantial energy and investment, and an increasing amount of land is being abandoned[31]. In the village of Amga in Yakutia, almost all of the arable land has been abandoned[32]. In Alaska, the land currently under cultivation accounts for less than 0.001% of the state's total land area[33]. One farmer in Alaska mentioned that they spend 20% of their annual budget on land reclamation to cope with the disruptions caused by permafrost[34]. The main reason for this situation is the disturbance to the ground surface induced by permafrost degradation, thereby adversely affecting crop cultivation, agricultural infrastructure, and machinery operations, and may even result in farmland abandonment[35]. Under the widespread influence of ground surface disturbance, even minor benefits, such as easily accessible water sources, are ultimately overshadowed[34].

To explore the dynamic relationship between permafrost and AF, as well as the potential impacts of permafrost on AF. Herein, we simulated the future suitability distributions of seven main crops (barley, maize, potato, soybean, sugarbeet, sunflower and wheat) across the global northern regions under two Shared

Socioeconomic Pathways (SSP1–2.6 and SSP5–8.5) scenarios, and projected permafrost degradation and its uncertainties. Subsequently, we assessed the spatial relationship between crop suitability and permafrost distribution during 1980–2010, 2041–2070, and 2071–2100. Finally, we developed a framework to quantify the potential influence of changing permafrost on the northward shift of AF. In doing so, we answered the following three questions: (i) How far will AF shift northward under continued climate warming? (ii) Does this shift occur faster than the retreat of permafrost, potentially leading to an overlap between climatically suitable agricultural zones and permafrost regions? (iii) How does permafrost degradation constrain the extent of potential future AF? This study enhances understanding of the northward expansion of AF under climate change by explicitly incorporating the influence of permafrost. It also provides practical insights for climate adaptation in northern communities.

Results

Model performance

We used the optimized Maximum Entropy (MaxEnt) machine-learning model to simulate the spatial distribution of suitability for seven major crops selected based on harvested area, crop types, yield, and energy contribution (see Methods: Main crops and occurrence data). Model performance was evaluated using the Area Under the Receiver Operating Characteristic Curve (AUC), which measures the model's ability to distinguish between presence and background samples (see Methods: Crop suitability modeling). The mean AUC of crops, calculated from ten repeated trials using a 25% validation set (independent of the 75% training data), ranged from 0.81 to 0.91 (Supplementary Figure 1, barley: 0.82, maize: 0.82, potato: 0.83, soybean: 0.89, sugar beet: 0.90, sunflower: 0.91, and wheat: 0.81), indicates that all MaxEnt simulations achieved good to excellent predictive performance[36,37]. The simulated crop suitability zones are often larger than the actual cultivated areas, because not all regions suitable for crop growth have been developed into cropland. As shown in Supplementary Figure 2, the spatial extent of single and limited double cropping zones (GAEZ v4[54]) is substantially larger than the current cropland coverage, with cropland accounting for 56% of the single and limited double cropping zones. The Kappa coefficient between them is 0.66. In contrast, our modeled crop suitability zone (at least one crop is suitable within a grid cell) yielded a more intermediate result: current cropland occupies 74% of our modeled suitable area, with a Kappa coefficient of 0.70. The total area of our modeled crop suitability zone represents 76% of the GAEZ-defined single and limited double cropping zones, and the Kappa coefficient between them is 0.78. In addition, the northern boundary of our modeled crop suitability zone closely aligns with that of current cropland, averaging at 57.10°N and 57.24°N, respectively, supporting the accuracy of our suitability boundary detection and its relevance to the change of permafrost (Supplementary Figure 2).

The MAAT-permafrost approach estimates the probability of near-surface permafrost occurrence for each grid cell from mean annual air temperature (MAAT), allowing the spatial distribution of permafrost to be derived (see Methods: Permafrost extent derivation and Post-modeling analysis). In the original methodological study[38], the estimated permafrost area was 15.5 million km², which compares well to observed value of 15.0 million km². This type of air–ground coupling approach for simulating permafrost extent generally performs better than other methods[39]. In our study, the simulated permafrost extent using the MAAT-permafrost approach for the baseline period (1980–2010, consistent with the baseline period used for crop suitability simulations) closely aligned with observations, yielding a Kappa coefficient of 0.90 (Supplementary Figure 3). Taken together, both the MaxEnt and MAAT-permafrost models produced reliable outputs, providing a robust foundation for the subsequent

analyses.

Northward shift of crop climatic suitability zones

Crop climatic suitability zones (hereafter referred to as CCSZ) were defined as grid cells in which at least one of the seven representative crops was classified as suitable (see Methods: Post-modeling analysis). Based on outputs from five Global Climate Models (GCMs) spanning an appropriate range of equilibrium climate sensitivity within the CMIP6 ensemble[40], we further examined changes in the spatial distribution of CCSZ during the mid- and late twenty-first century. By the end of the 21st century (2071–2100) under the SSP5–8.5 scenario, the northern boundary of CCSZ shifted northward by an average of 739 km compared to the baseline period, with a range of 583 to 1552 km across different GCMs, indicating substantial inter-model variability (Fig. 1a). Using area-weighted calculations, we determined the latitudinal centroids of suitable areas for each crop, all of which exhibited a clear northward shift (Fig. 1b). On GCMs model average, the centroid of CCSZ advanced northward by 586 km, with individual crops showing the following shifts: barley, 718 km; maize, 387 km; potato, 602 km; soybean, 898 km; sugarbeet, 604 km; sunflower, 462 km; and wheat, 534 km. The total area of projected AF reaches approximately 11.64 million km², (for scale, equivalent to over 24% of the current agricultural land[41], Fig. 1).

Results across periods and scenarios consistently indicate the emergence of AF in the future. By the end of the century under the SSP1–2.6 scenario, the northern boundary of CCSZ shifts northward by an average of 331 km (290–685 km across different GCMs). The centroid of CCSZ moves northward by 248 km, with individual crops showing the following shifts: barley, 278 km; maize, 177 km; potato, 263 km; soybean, 414 km; sugarbeet, 249 km; sunflower, 220 km; and wheat, 222 km. The area of AF reaches 4.86 million km² (for scale, ~10% of current agricultural land; Supplementary Figure 6). By mid-century, AF is projected to amount to at least 10% of current agricultural land (Supplementary Figures 4–5), reaching 4.90 million km² under SSP1–2.6 and 7.40 million km² under SSP5–8.5 during 2041–2070, the northern boundary of CCSZ shifts northward by an average of 342 km and 482 km, respectively.

Coexistence of CCSZ and permafrost regions

Future warming simultaneously drives the northward shift of CCSZ boundaries and the retreat of the southern limit of permafrost. While, this synchronous change does not appear to expand the overlap between CCSZ and permafrost regions. Notably, permafrost degradation remains highly uncertain under comparable warming levels[42–44]. Therefore, we aim to examine whether the sensitivity of permafrost to warming (manifested as differences in the rate and extent of degradation under the same level of warming) may lead to greater spatial coexistence between permafrost regions and CCSZ. We applied the MAAT-permafrost approach to simulate permafrost dynamics, yielding a best-fit estimate (i.e., the closest agreement between simulated and observed extent) and two end-member cases representing minimum and maximum permafrost retention under the same warming level (see Methods: Permafrost extent derivation). To obtain quantitative estimates and avoid confounding among permafrost cases and climate models, we used the ensemble mean of five GCMs to assess the spatial relationship between permafrost and CCSZ.

The coexistence between permafrost regions and CCSZ occurs primarily along the southern margin of the permafrost zone. In the baseline period, the overlap is approximately 0.94 million km² (5% of CCSZ; Fig. 2a). Despite the northward shift of CCSZ and the southward retreat of permafrost, the overlap increases only slightly to 1.19 million km² under SSP5–8.5 during 2071–2100 in the best-fit case (5% of CCSZ; Fig. 2b). In contrast,

it expands markedly to 4.43 million km² under the maximum case (17% of CCSZ; Fig. 2d), approximately five times the baseline, but declines to 0.86 million km² under the minimum case (3% of CCSZ; Fig. 2c). Under SSP1–2.6, the overlap is slightly greater than under SSP5–8.5, reaching 1.35 million km² (5% of CCSZ) in the best-fit case, increasing to 4.65 million km² (19%) under the maximum case, and decreasing to 1.04 million km² (4%) under the minimum case (Supplementary Figure 7). Across time periods, variation in overlap is primarily driven by uncertainty in permafrost degradation (Supplementary Figure 8), with most co-occurring areas located in regions of sporadic and isolated permafrost (Permafrost can be classified into four categories according to its areal continuity: continuous (>90%), discontinuous (50–90%), sporadic (10–50%), and isolated patches (<10%)[45]).

Ground ice content of AF

Ground ice content data were obtained from the National Snow and Ice Data Center (NSIDC)[45], a dataset widely used in studies of permafrost change and its impacts[46–48]. This dataset provides ground ice content in three categories—high, medium, and low—corresponding to >20%, 10–20%, and <10% ice by soil volume, respectively. As shown in Fig. 3, we quantified the proportion of AF that were historically underlain by near-surface permafrost, along with the ground ice content, providing a basis for further assessing the influence of permafrost on AF (detailed in Discussion: How permafrost affects AF?).

By the end of the century under the SSP5–8.5 scenario, approximately 69% of the AF in North America are projected to emerge from areas formerly characterized by permafrost (best-fit permafrost case). Among these, regions with high ground ice content contribute a relatively small proportion (2% of AF), while medium and low ground ice content areas account for 16% and 51% of AF, respectively. In Eurasia, about 73% of AF are projected to originate from permafrost zones. Unlike North America, a higher proportion of AF in Eurasia emerges from high ground ice content areas (15% of AF), whereas medium ground ice content areas contribute the least (6% of AF) and low ground ice content areas account for the largest share (52% of AF) (Fig. 3). Under the SSP1–2.6 scenario, 48% and 59% of AF in North America and Eurasia, respectively, originate from areas formerly underlain by permafrost. In North America, regions of high, medium, and low ground ice content account for 0%, 10%, and 38% of AF converted from permafrost, respectively. In Eurasia, the corresponding proportions are 13%, 3%, and 43%. By mid-century, more than half of AF is also projected to emerge from areas formerly underlain by permafrost (Supplementary Figures 9–10), with only minor differences in the contributions from regions of different ground ice content compared to the end of the century.

An integrated permafrost-informed crop suitability map

As shown in Fig. 4, based on the multi-GCM ensemble mean and the best-fit permafrost case, we have overlaid the results from three dimensions: the suitability of seven representative crops, near-surface permafrost dynamics, and ground ice content. First, AF is classified into six mutually exclusive categories based on near-surface permafrost dynamics (presence or absence) and ground ice content. By the end of the century, under the SSP5–8.5 scenario: Cat. 1: AF converted from non-permafrost regions (23% of AF). Cat. 2: AF converted from low-ice-content permafrost regions, with near-surface permafrost completely thawed in the simulations (49% of AF). Cat. 3: AF converted from medium-ice-content permafrost regions, with near-surface permafrost completely thawed in the simulations (9% of AF). Cat. 4: AF coexists with sporadic and isolated permafrost, where near-surface permafrost persists in the simulations (9% of AF). Cat. 5: AF converted from high-ice-content permafrost regions, with near-surface permafrost completely thawed in the simulations (9% of AF). Cat. 6: AF coexists with

continuous and discontinuous permafrost, where near-surface permafrost persists in the simulations (<1% of AF).

Second, we overlay the six categories with crop suitability abundance, defined as the number of crops classified as suitable by the MaxEnt model within each grid cell. Areas with crop abundance levels from 1 to 7 account for 20%, 14%, 18%, 22%, 14%, 9%, and 3% of AF, respectively. Finally, AF is subdivided into 42 sub-regions, with the area and proportion of each shown in Fig. 4 and Table 1. By the end of the century under the SSP1–2.6 scenario, Cat. 1–6 account for 39%, 29%, 4%, 19%, 6%, and 4% of AF, respectively, while crop abundance levels 1–7 account for 27%, 22%, 28%, 18%, 4%, 1%, and <1% of AF. These results indicate that lower levels of warming are associated with an overall reduction in crop abundance and greater coexistence of AF with permafrost (Supplementary Figure 13 and Supplementary Table 3). The same approach was applied to the mid-century period, and the results, as well as the spatial distribution and extent of the sub-regions under the SSP5–8.5 and SSP1–2.6 scenarios, are shown in Supplementary Figures 11–12 and Supplementary Tables 1–2.

Discussion

How permafrost affects AF?

By the end of the century under the SSP5–8.5 scenario, most AF (77%) originates from areas that were underlain by permafrost during the baseline period (Cat. 2–6), whereas only 23% of AF is unaffected by permafrost (Cat. 1). Within the 59% of AF derived from low- and medium-ground-ice-content regions (Cat. 2 and Cat. 3), near-surface permafrost has completely thawed, suggesting that additional management efforts, such as land leveling and drainage, may be required to mitigate residual impacts of permafrost degradation, including surface water accumulation[46], ground subsidence[49], and thermokarst gullies and slumping[50]. Approximately 9% of AF coincides with sporadic and isolated permafrost (Cat. 4), where near-surface permafrost remains relatively warm, highly dynamic, and spatially unpredictable, representing degradation hotspots[51]. Even after land leveling, residual permafrost may continue to thaw, and sustaining cultivation in these areas could require ongoing management to cope with unpredictable ground surface changes[32,34,35]. Another 9% of AF originates from high-ground-ice-content permafrost regions (Cat. 5), where complete thawing of near-surface permafrost may lead to strong ground surface disturbances[52]. Such disturbances could incur prohibitively high costs to render the land cultivable, and extensive ground subsidence could hinder agricultural machinery operations, potentially resulting in farmland abandonment[35,53]. Less than 1% of AF coexists with continuous and discontinuous permafrost (Cat. 6), which is generally considered unsuitable for cultivation[54].

For now, at least 9% of AF (Cat. 5 and Cat. 6) is rendered unsuitable for cultivation due to the influence of permafrost. Notably, AF coexisting with sporadic and isolated permafrost (Cat. 4, 9% of AF) is primarily located along the northern margins of AF (Fig. 4), where population density is low[55] and growing degree days are limited[56], both of which are key factors influencing crop cultivation. In addition, most of this region is projected to support fewer than three crops (81% of Cat. 4; Fig. 4 and Table 1). Based on the limited evidence currently available, the coexistence of thawing near-surface permafrost and AF appears to be dominated by negative impacts on agricultural production[32,34,57,58]. Consequently, considering the harsher climate conditions along the northern margins and the limited potential returns, combined with the ongoing negative impacts and management costs associated with continued permafrost degradation, this type of AF may not be economically viable for cultivation. In total, 18% of AF (Cat. 4, Cat. 5, and Cat. 6) appears to be dominated by the negative effects of permafrost and may even be unsuitable for conversion to arable land.

By the end of the century, under the SSP1–2.6 scenario (Supplementary Figure 13 and Supplementary Table

3), Cat. 4, Cat. 5, and Cat. 6 account for 19%, 6%, and 4% of AF, respectively, indicating that 29% of AF is primarily dominated by the negative effects of permafrost. This is largely driven by the expansion of Cat. 4, as lower warming allows more subsurface ice in near-surface permafrost to be preserved, while crops cultivated above ground are more sensitive to temperature increases, resulting in a greater coexistence of AF with near-surface permafrost. By mid-century, simulated AF under the SSP1–2.6 and SSP5–8.5 scenarios amounts to 4.90 million km² and 7.40 million km², respectively. Under the same assumptions, the proportion of AF primarily dominated by the negative effects of permafrost is 27% and 24%, respectively (Supplementary Figures 11–12 and Supplementary Tables 1–2).

Uncertainties imposed by permafrost on AF

Permafrost continues to degrade under ongoing climate warming. Recent studies suggest that, at large spatial scales, permafrost thaw exhibits an approximately linear relationship with temperature increases[48]. However, substantial differences remain in both the magnitude and timing of projected changes[42]. Projections from CMIP6 models indicate that for every 1 °C increase in global mean surface temperature, the annual volume of frozen ground in the upper 2 meters of soil may decrease by 10% to 40%[43]. Considerable uncertainty persists in future projections of permafrost extent: under the RCP8.5 scenario, permafrost losses between 2010 and 2299 range from 6 to 16 million km²[44].

In our study, the MAAT-permafrost approach captured the upper and lower bounds of permafrost degradation under a given level of warming[38], reflecting the sensitivity of permafrost to warming (see Results: Coexistence of CCSZ and permafrost regions). We integrated this range into the crop comprehensive suitability map (using the same method as described in Results: An integrated permafrost-informed crop suitability map) to further discuss the uncertainties imposed by permafrost on AF. As shown in Table 1 (values in parentheses), by the end of the century under the SSP5–8.5 scenario, the minimum and maximum extents of near-surface permafrost drive substantial transitions between Cat. 2 and Cat. 4 within AF. The extent of Cat. 4 ranges from 7% to 36% of AF, indicating that the lower and upper bounds of permafrost degradation correspond to 7–36% of AF coexisting with near-surface sporadic and isolated permafrost. If Cat. 4, Cat. 5, and Cat. 6 are all considered as areas not recommended for conversion to arable land, then 16–42% of AF may be primarily dominated by the negative effects of permafrost. Under the SSP1–2.6 scenario, Cat. 4, Cat. 5, and Cat. 6 collectively account for 25–65% of AF. The upper bound of this range is substantially higher than that under the SSP5–8.5 scenario. Notably, the maximum values discussed here represent extreme upper estimates derived from the maximum permafrost case, whereas actual conditions are likely closer to those obtained under the best-fit scenario (see Discussion: How permafrost affects AF?). By mid-century, the proportion of AF primarily dominated by the negative effects of permafrost ranges from 24% to 62% under SSP1–2.6 and from 21% to 52% under SSP5–8.5 (Supplementary Tables 1–2).

Moreover, several factors still contribute to additional uncertainty regarding the impacts of permafrost on AF. For instance, current models largely focus on near-surface permafrost (upper 3 m of the subsurface[42,44,59]), whereas deeper permafrost (5–10 m and below) may persist for decades even after surface thaw. Agricultural expansion often occurs near river valleys[60], where ice-rich permafrost is also commonly concentrated, yet existing hemispheric ground ice datasets[45,61] lack the detail to capture these environments. From these factors, permafrost may exert additional negative effects on AF, most of which (77%) originate from areas underlain by permafrost during the baseline period (Cat. 2–6). Conversely, the thawing of permafrost may increase surface

water and soil moisture, potentially providing a temporary water supply to originally arid AF regions[34]. In addition, these previously cold areas may have accumulated a certain amount of fertile soil[62,63]. Although these factors appear beneficial, the extent to which such limited advantages can offset the negative impacts of permafrost change and the associated potential economic costs remains highly uncertain and complex.

Limitations and implications

Species' ecological niches and crop suitability should be assessed over defined periods, as both require time to respond to climate change rather than adjusting instantly to interannual variability. This study evaluated representative crop suitability for the mid- and late 21st century using 30-year climate means to represent stable climatic states. Simulated permafrost dynamics are similarly based on 30-year means. However, at regional and short temporal scales, predicting permafrost changes remains highly uncertain due to limited observations and complex responses[17]. Transitions from permafrost to stable agricultural land involve thermokarst-induced processes such as subsidence, waterlogging, and subsequent drainage[40,49,50], whose timing, location, and magnitude are difficult to predict at large scales[17]. Limitations also exist in capturing sub-annual variability and crop phenology[64], and the relationship between warming and Northern Hemisphere vegetation productivity may reverse in the future[65]. Consequently, interannual lags between permafrost degradation and crop suitability remain challenging to capture. Regional-scale studies are therefore necessary to resolve finer-scale complexities. Detailed regional models and field studies are needed to examine the links between ground ice content and thermokarst formation, tolerable ice loss for agriculture, permafrost–surface water interactions[47], human decision-making and societal development[66], and coupled water–nutrient dynamics in permafrost[67]. Even where climate appears suitable, the transition from potential to realized crop cultivation remains uncertain, requiring adaptive assessment by local communities using local knowledge and continued regional-scale research[8,68].

Permafrost thaw profoundly affects Indigenous peoples and traditional livelihoods in the Arctic, with most attention focusing on its negative impacts. These can be summarized as: infrastructure failure, disruption of mobility and supplies, challenges to food security, declines in water quality, and exposure to infectious diseases and contaminants[69]. Among these, threats to food security are considered a major permafrost-related hazard in some self-sufficient northern communities[69]. These challenges arise from biodiversity loss, habitat degradation, declines in animal populations[70], and negative impacts on traditional subsistence activities, including fishing, reindeer herding, hunting, and associated cultural and spiritual practices. Our results indicate that, although climate-driven AF is constrained by permafrost and the process is highly complex, future warming is likely to continue creating new crop-suitable areas for Arctic communities. In the current context, dominated by negative impacts, this may provide novel opportunities for local adaptation to climate change. Accordingly, raising awareness of climate change within communities and encouraging farmers to adapt to longer growing seasons (for example, by selecting crop varieties suited to local conditions[71]) is important. Policymakers should consider the potential landscape changes induced by climate change when formulating long-term socio-economic strategies[72]. Future research should continue to explore how local residents perceive and experience cryospheric changes[73]. By integrating indigenous cumulative local knowledge, interdisciplinary field studies can investigate the feasibility and practicalities of cultivation in thawing permafrost regions, thereby leveraging the benefits of warming to mitigate its negative impacts.

Currently, the agricultural expansion[8,9] is raising widespread concerns over a potential land conflict between agriculture and timber production[74]. However, our findings suggest that when accounting for the impacts of

permafrost, approximately 18% to 29% of the projected AF may become unsuitable for cultivation in high-latitude regions. Moreover, permafrost soils store vast quantities of organic carbon, and the carbon loss following deforestation for agriculture is strongly dependent on permafrost abundance[75]. Converting forested land to cropland in permafrost regions may further accelerate thawing and lead to substantial carbon emissions. In addition, if the minimum land area required to safeguard biodiversity is considered[6], the effective extent of the AF would be further reduced. Consequently, our findings may partially alleviate concerns regarding land-use conflicts between agriculture and forestry, while simultaneously underscoring the urgent need to reduce emissions, enhance agricultural efficiency, and invest in sustainable intensification within existing cropland boundaries as key strategies for ensuring global food security.

Methods

Study area

The study area encompasses all terrestrial regions of the Northern Hemisphere between 30°N and 83°N, providing a suitable spatial extent for examining large-scale relationships between the northward shift of agricultural suitability zones and permafrost dynamics (Supplementary Figure 14). The southern boundary was set at 30°N because this range includes all high-latitude permafrost regions in the Northern Hemisphere, as well as the majority of areas characterized by single cropping and limited double cropping zones. In future forecasts, agricultural suitability is projected to increase substantially in high-latitude regions, whereas the increment in high-altitude areas is comparatively negligible[2].

Main crops and occurrence data

To identify representative crops that effectively capture the northern boundary of crop climatic suitability zones, we compiled harvested area data for 175 crops[76] within single-cropping and limited double-cropping regions north of 30°N. After excluding crops accounting for less than 1% of the total harvested area, 14 major crops remained for further analysis (Supplementary Figure 15). According to the objectives of this study, forage crops were excluded, and efforts were made to include a wide range of crop types to capture the distinct environmental requirements of different crop groups. Additionally, crop selection was informed by yield and energy contribution (excluding crops with relatively low yields or limited energy contribution, FAOSTAT[77], https://www.fao.org/). Finally, we selected seven major crops to analyze the northward shift of AF: three cereals (wheat, maize, and barley), two oil crops (soybean and sunflower), one sugar crop (sugarbeet), and one root and tuber crop (potato). This selection covers four out of five the most valuable crops globally according to the FAO (rice, maize, wheat, soy, and potato).

It is necessary to create an observation-based, real-world dataset to model and validate the accuracy of our models. As species distribution models require that occurrence data be unbiased and not extend beyond or lie too close to the temporal bounds of the climate data, we used three harvested area datasets around the year 2000 to generate the occurrence data and reduce the bias of a single data source while ensuring consistency among climate datasets. These datasets include the Global Data Set of Monthly Irrigated and Rainfed Crop Areas around the year 2000 (MIRCA2000[78]), the Spatial Production Allocation Model (SPAM; https://mapspam.info), and Harvested Area and Yield for 175 Crops from EARTHSTAT[76]. It was considered that harvested area fractions below 1% were not suitable for planting[79]. Therefore, all grid cells with harvested area fractions below 1% were excluded, and the spatial resolution and units of the three datasets were harmonized. To reduce biases in

occurrence data, the three harvested area datasets were overlaid (with spatially overlapping points retained), and a variable-sized moving window was slid across the entire dataset. Within each window position, one data point was randomly selected from the three sources and retained as the sole occurrence within that area. After traversing the entire dataset, this procedure yielded an occurrence database with reduced bias from any single data source and a more even spatial distribution with fewer records[80]. To exclude the influence of tropical and subtropical crop varieties, occurrences were retained only within single cropping and limited double cropping zones north of 30°N. The number of occurrences per crop was initially 175637–26561 and was then thinned to 1179–1656. (Supplementary Figure 16).

Environmental input data: Present and climate change projections

Climate data were obtained from the CHELSA Version 2.1 (Climatologies at High Resolution for the Earth's Land Surface Areas) climate dataset at 30 arc-second resolution[81]. In addition to the 19 bioclimatic variables commonly used in species distribution modeling[82,83], 20 additional crop-related climate variables were also collected (Supplementary Table 4). These climatological variables, together with the other variables mentioned below, were then subjected to pre-modeling selection to identify the most important predictors. All climate variables represent multi-year averages for three time periods: the historical baseline period (1980–2010) and two future periods (mid-century: 2041–2070; end-century: 2071–2100).

In this study, we selected climate variables from five CMIP6 GCMs: GFDL-ESM4, MPI-ESM1-2-HR, MRI-ESM2-0, IPSL-CM6A-LR, and UKESM1-0-LL. We considered two Shared Socioeconomic Pathways (SSPs), SSP1–2.6 and SSP5–8.5, to capture the full range of projected crop suitability changes. The five selected GCMs feature structurally independent ocean–atmosphere components and together span the appropriate range of equilibrium climate sensitivity (ECS) represented in the CMIP6 ensemble. This includes three models with below-average ECS values (GFDL-ESM4, MPI-ESM1-2-HR, and MRI-ESM2-0) and two with above-average ECS values (IPSL-CM6A-LR and UKESM1-0-LL)[40].This model ensemble has been widely applied in studies related to agriculture and climate change[16].

Soil data were obtained from HWSD 2.0 (https://gaez.fao.org/pages/hwsd), including 14 variables (see Supplementary Table 4). Nine topographic variables (Supplementary Table 4) were sourced from EarthEnv (https://www.earthenv.org/). One groundwater table depth variable was obtained from a published study[84], which integrates previous studies by averaging four commonly used datasets (Supplementary Table 4). In total, 63 environmental variables were used to calculate crop suitability. All variables were spatially aligned to the extent of the study area (Supplementary Figure 14) and resampled to a uniform spatial resolution of 5 arc minutes (approximately 10 km at the equator).

Observed permafrost extent and ground ice content data were obtained from the National Snow and Ice Data Center (NSIDC), which is a widely used dataset in studies analyzing permafrost changes and their impacts[46–48]. The distribution of global single and limited double cropping zones during the historical period was derived from the Global Agro-Ecological Zones model (GAEZ v4, https://www.fao.org/gaez/en/) and was used to filter occurrences. Crop yield and caloric contribution data were sourced from FAOSTAT[77] (https://www.fao.org/), and cropland distribution data were obtained from FAO (https://www.fao.org/) to validate model accuracy.

Crop suitability modeling

MaxEnt version 3.4.4[85] (https://biodiversityinformatics.amnh.org/open_source/maxent/) was used to simulate

the current and future spatial suitability distributions of seven selected crops (wheat, maize, barley, soybean, sunflower, sugarbeet, and potato). MaxEnt was chosen for its robustness and high predictive accuracy, which has led to its widespread application in modeling the distributions of a variety of species, including crops[86–88], vegetation[89,90], animals[82,83,91], insects[92], and microorganisms[93]. The model has consistently exhibited high predictive accuracy[94] compared with other species distribution models. For each crop, first, we conducted a variable selection from the 63 environmental variables. Pairwise spatial correlations between all variables were calculated. Then, among the 25 spatially independent variables, those with permutation importance consistently above 1% across multiple MaxEnt runs were retained as base variables. The non-base variables were then individually modeled in combination with the base variables, and their permutation importance was calculated. Based on the ranked permutation importance of the non-base variables and their spatial correlations with other variables, those with higher importance were prioritized, while highly correlated variables with them ($r > 0.8$) were excluded. The selected variables from this round were combined with the base variables for another round of modeling, during which variables with permutation importance below 1% were removed. This process was iteratively repeated until all retained variables had a permutation importance greater than 1%. The final set of variables used for model construction is summarized in Supplementary Table 4.

The selected variables were used for optimal model selection with the ENMeval package v2.0.5[95], in R, v4.4.2 (R Core Team, 2024). Five feature classes (FCs: Linear, Quadratic, Product, Hinge, and Threshold) were combined with regularization multipliers (RM, integers from 1 to 5 in this study), resulting in 25 parameter combinations. The optimal model was selected based on the criterion of delta AICc = 0, which indicates that MaxEnt achieves a good balance between model fit and complexity, thereby minimizing the risk of overfitting[95–97]. Subsequently, for each crop, 100 null models were generated under the optimal model settings. A model was confirmed as optimal only if its AUC exceeded that of 99% of the null models. Otherwise, the above procedures were repeated until the model passed the null model test.

Finally, the optimized models were used to project the suitability distributions for different crops across three time periods—Baseline (1980–2010), mid-century (2041–2070), and end-century (2071–2100)—under two SSPs (SSP1–2.6 and SSP5–8.5) and five GCMs (GFDL-ESM4, IPSL-CM6A-LR, MPI-ESM1-2-HR, MRI-ESM2-0, and UKESM1-0-LL), for a total of seven crops. Each modeling run was repeated ten times (10-fold cross-validation), with 75% of the data used for training and 25% for validation in each run. Model performance was evaluated using AUC value, which was categorized into five classes: failed (0.5–0.6), poor (0.6–0.7), fair (0.7–0.8), good (0.8–0.9), and excellent (0.9–1)[36]. If the training AUC of a model was below 0.8, all procedures were repeated until the model reached a good or excellent level.

Permafrost extent derivation

The extent of near-surface permafrost (within the upper 3 m of the subsurface) was derived following previously established procedures[38], updated from earlier work[98]. In this approach, the probability of near-surface permafrost occurrence is represented as a cumulative normal distribution function of the mean annual air temperature (MAAT) at each grid cell. This model is designed to simulate permafrost extent under specific temperature increase scenarios or time periods in a climatically stable state. This model performs well in simulating the spatial extent of near-surface permafrost and effectively captures the lagged response of permafrost degradation relative to climate change[38], and provides estimates of the uncertainty in future permafrost dynamics, including a best-fit case, which represents the modeled permafrost extent most closely

aligned with observational data, and maximum/minimum cases, which represent the upper and lower bounds of simulated permafrost extent. This allows us to analyze the impact of such uncertainties on crop suitability zones and has been widely applied in studies on permafrost degradation and its derived impacts[43,48,99].

Post-modeling analysis

The MaxEnt output represents the probability of species presence at a given location under the corresponding model input conditions, ranging from 0 to 1. We applied a Maximum Test Sensitivity Plus Specificity (MTSPS) threshold[100] to convert the continuous MaxEnt outputs into binary classifications of suitable and unsuitable areas. Subsequently, binary suitability maps of the seven crops were overlaid to generate one crop suitability map, which integrates the distinct environmental requirements of different crop types. For each crop, the final suitability map was derived from an ensemble average across 5 GCMs. A grid cell was considered climatically suitable for agriculture if at least one crop was classified as suitable, and these grid cells were collectively defined as crop climatic suitability zones (CCSZ). AF was then defined as grid cells classified as unsuitable in the historical period but projected to become suitable in the future. This allowed us to identify and characterize the potential northern boundary of agricultural suitability under climate change.

The MAAT-permafrost model outputs the probability of near-surface permafrost presence at each grid cell. First, cells with a permafrost probability below 0.01 were classified as non-permafrost areas[81]. Cells with probabilities between 0.9–1.0, 0.5–0.9, 0.1–0.5, and 0–0.1 were classified as continuous, discontinuous, sporadic, and isolated patches of permafrost, respectively[99]. To ensure the robustness of our simulation results, we used the Kappa coefficient to assess spatial agreement between (i) the simulated crop suitability map and the observed extent of single and limited double cropping zones as well as cropland cover in baseline period, and (ii) the simulated permafrost extent and the observed permafrost distribution. Changes in the spatial distribution of crop suitability and the influence of permafrost on these changes were assessed by comparing suitability maps with permafrost maps for each scenario and time period. Modeling and post-modeling analyses were conducted using R v4.4.2 (R Core Team[101]) and MATLAB R2022a (academic use) (MathWorks[102]).

Data availability

All data used in this study are publicly available. Harvested-area data were obtained from MIRCA2000 (https://www.uni-frankfurt.de/45218031/MIRCA2000), SPAM (https://mapspam.info), and EARTHSTAT (http://www.earthstat.org/harvested-area-yield-175-crops/). Climate data were obtained from CHELSA Version 2.1 (https://chelsa-climate.org/downloads/). Soil data were obtained from HWSD 2.0 (https://gaez.fao.org/pages/hwsd). Topographic data were obtained from EarthEnv (https://www.earthenv.org/). Groundwater table depth data were obtained from a published dataset (https://zenodo.org/records/7538161). Observed permafrost extent and ground ice content data were obtained from NSIDC (https://nsidc.org/data/ggd318/versions/2). The distribution of global single and limited double cropping zones during the historical period was derived from GAEZ v4 (https://www.fao.org/gaez/en/). Crop yield, caloric contribution, and cropland distribution data were obtained from FAOSTAT (https://www.fao.org/faostat/). Source data underlying the main findings of this study are available at Zenodo (https://doi.org/10.5281/zenodo.20282716).

Code availability

Custom code for species occurrence point filtering and permafrost distribution simulation is available at Zenodo (https://doi.org/10.5281/zenodo.20282716). Species distribution modeling was conducted using the publicly available MaxEnt version 3.4.4 (https://biodiversityinformatics.amnh.org/open_source/maxent/) and the publicly available R package ENMeval v2.0.5 (https://cran.r-project.org/package=ENMeval).

References

1. Zabel, F., Putzenlechner, B. & Mauser, W. Global Agricultural Land Resources—A High Resolution Suitability Evaluation and Its Perspectives until 2100 under Climate Change Conditions. PLoS ONE 9, e114980 (2014).
2. King, M. et al. Northward shift of the agricultural climate zone under 21st-century global climate change. Sci. Rep-Uk 8, 7904 (2018).
3. Hannah, L. et al. The environmental consequences of climate-driven agricultural frontiers. PLoS ONE 15, e0228305 (2020).
4. Foley, J. A. et al. Solutions for a cultivated planet. Nature 478, 337–342 (2011).
5. Forslund, A. et al. Can healthy diets be achieved worldwide in 2050 without farmland expansion? Glob. Food Secur-Agr. 39, 100711 (2023).
6. Allan, J. R. et al. The minimum land area requiring conservation attention to safeguard biodiversity. Science 376, 1094-1101 (2022).
7. Kloffel, T. et al. The challenges fraught opportunity of agriculture expansion into boreal and Arctic regions. Agr. Syst. 203, 103507 (2022).
8. Meyfroidt, P. Emerging agricultural expansion in northern regions: Insights from land-use research. One Earth 4, 1661–1664 (2021).
9. Bradley, H. & Stein, S. Climate opportunism and values of change on the Arctic agricultural frontier. Econ. Anthropol. 9, 207–222 (2022).
10. Lobell, D. B. & Di Tommaso, S. A half- century of climate change in major agricultural regions: Trends, impacts, and surprises. P. NATL. ACAD. SCI. USA. 122, e2502789122 (2025).
11. Challinor, A. J. et al. A meta-analysis of crop yield under climate change and adaptation. Nat. Clim. Change 4, 287–291 (2014).
12. Rezaei, E. E. et al. Climate change impacts on crop yields. Nat. Rev. Earth. Env. 4, 831–846 (2023).
13. Mombo, V.-G. et al. Have crops already reached peak suitability: Assessing global climatic suitability decreases for crop cultivation. Environ. Res. Lett. 20, 034009 (2025).
14. Heikonen, S. et al. Climate change threatens crop diversity at low latitudes. Nat. Food 6, 331–342 (2025).
15. Kornhuber, K. et al. Risks of synchronized low yields are underestimated in climate and crop model projections. Nat. Commun. 14, 3528 (2023).
16. Jagermeyr, J. et al. Climate impacts on global agriculture emerge earlier in new generation of climate and crop models. Nat. Food 2, 873–885 (2021).
17. Calvin, K. et al. Climate Change 2023: Synthesis Report. Contribution of Working Groups I, II and III to the Sixth Assessment Report of the Intergovernmental Panel on Climate Change [Core Writing Team, H. Lee and J. Romero (eds.)]. IPCC, Geneva, Switzerland. Intergovernmental Panel on Climate Change (IPCC) (2023).
18. Feng, L. et al. Globally increased cropland soil exposure to climate extremes in recent decades. Nat. Commun. 16, 4354 (2025).
19. Hasegawa, T. et al. Extreme climate events increase risk of global food insecurity and adaptation needs. Nat. Food 2, 587–595 (2021).

20. Liu, B. et al. Co-benefits for net carbon emissions and rice yields through improved management of organic nitrogen and water. Nat. Food 5, 241–250 (2024).
21. Fujimori, S. et al. Land-based climate change mitigation measures can affect agricultural markets and food security. Nat. Food 3, 110–121 (2022).
22. Gao, P. et al. Heterogeneous pressure on croplands from land-based strategies to meet the 1.5 °C target. Nat. Clim. Change 15, 420–427 (2025).
23. Grados, D. et al. Common agronomic adaptation strategies to climate change may increase soil greenhouse gas emission in Northern Europe. Agr. Forest Meteorol. 349, 109966 (2024).
24. McClelland, S. C. et al. Managing for climate and production goals on crop-lands. Nat. Clim. Change 15, 642–649 (2025).
25. Hultgren, A. et al. Impacts of climate change on global agriculture accounting for adaptation. Nature 642, 644–652 (2025).
26. Unc, A. et al. Expansion of Agriculture in Northern Cold-Climate Regions: A Cross-Sectoral Perspective on Opportunities and Challenges. Frontiers in Sustainable Food Systems 5, 663448 (2021).
27. Chaloner, T. M., Gurr, S. J. & Bebber, D. P. Plant pathogen infection risk tracks global crop yields under climate change. Nat. Clim. Change 11, 710–715 (2021).
28. Tchebakova, N. M. et al. Agroclimatic potential across central Siberia in an altered twenty-first century. Environ. Res. Lett. 6, 045207 (2011).
29. Bahadur, K. K. C. et al. Opportunities and trade-offs for expanding agriculture in Canada's North: An ecosystem service perspective. Facets 6, 1728–1752 (2021).
30. Franke, J. A. et al. Agricultural breadbaskets shift poleward given adaptive farmer behavior under climate change. Glob. Change Biol. 28, 167–181 (2022).
31. Danilova, L.I., Nikiforov, A.G. & Byastinova, L.M. Agricultural Development of the Republic of Sakha (Yakutia) on Permafrost. Proceeding of the International Science and Technology Conference "FarEastCon 2021" 967–980 (2022).
32. Lytkin, V. et al. Influence of Permafrost Landscapes Degradation on Livelihoods of Sakha Republic (Yakutia) Rural Communities. Land 10, 101. (2021).
33. Parlato, N. J. & Jones, M. W. The law of thaw: Understanding subnational land use policies for permafrost-agroecosystems. Polar Rec., 61, e3 (2025).
34. Jones, M. W. et al. Socioecological dynamics of diverse global permafrost-agroecosystems under environmental change. Arct. Antarct. Alp. Res. 56, 2356067 (2024).
35. Ward Jones, M. K. et al. Climate-driven expansion of northern agriculture must consider permafrost. Nat. Clim. Change 12, 699–703 (2022).
36. Swets, J.A. Measuring the accuracy of diagnostic systems. Science 240, 1285–1293 (1988).
37. Jimenez-Valverde, A. Insights into the area under the receiver operating characteristic curve (AUC) as a discrimination measure in species distribution modelling. Global Ecol. Biogeogr. 21, 498–507 (2012).
38. Chadburn, S. E. et al. An observation-based constraint on permafrost loss as a function of global warming. Nat. Clim. Change 7, 340–344 (2017).
39. Steinert, N.J. et al. Evaluating permafrost definitions for global permafrost area estimates in CMIP6 climate models. Environ. Res. Lett. 19, 014033 (2024).
40. Meehl, G. A. et al. Context for interpreting equilibrium climate sensitivity and transient climate response from the CMIP6 Earth system models. Sci. Adv. 6, eaba1981 (2020).
41. FAO. Land statistics 2001–2023 – Global, regional and country trends. FAOSTAT Analytical Briefs, No.107. Rome (2025).
42. Smith, S. L. et al. The changing thermal state of permafrost. Nat. Rev. Earth. Env. 3, 10–23 (2022).

43. Burke, E. J., Zhang, Y. & Krinner, G. Evaluating permafrost physics in the Coupled Model Intercomparison Project 6 (CMIP6) models and their sensitivity to climate change. Cryosphere 14, 3155–3174 (2020).
44. McGuire, A. D. et al. Dependence of the evolution of carbon dynamics in the northern permafrost region on the trajectory of climate change. P. NATL. ACAD. SCI. USA. 115, 3882–3887 (2018).
45. Brown, J. et al. Circum-Arctic Map of Permafrost and Ground-Ice Conditions v.2 (NSIDC, accessed October 2024).
46. Jones, B.M. et al. Lake and drained lake basin systems in lowland permafrost regions. Nat. Rev. Earth. Env. 3, 85–98 (2022).
47. Webb, E. E. et al. Permafrost thaw drives surface water decline across lake-rich regions of the Arctic. Nat. Clim. Change 12, 841–846 (2022).
48. Nitzbon, J. et al. No respite from permafrost-thaw impacts in the absence of a global tipping point. Nat. Clim. Change 14, 573–585 (2024).
49. Zhang, T. et al. 2022. Warming-driven erosion and sediment transport in cold regions. Nat. Rev. Earth. Env. 3, 832–851 (2022).
50. Jiang, G. et al. Thaw slumps alter ecosystem carbon budget in alpine grassland on the Tibetan Plateau. Nat. Commun. 17, 190 (2026).
51. Li, X. et al. Unstable permafrost regions experience more severe heatwaves in a warming climate. npj Clim. Atmos. Sci. 8, 147 (2025).
52. Nitze, I. et al. Remote sensing quantifies widespread abundance of permafrost region disturbances across the Arctic and Subarctic. Nat. Commun. 9, 5423 (2018).
53. Desyatkin, R. et al. Degradation of Arable Soils in Central Yakutia: Negative Consequences of Global Warming for Yedoma Landscapes. Frontiers in Earth Science 9, 683730 (2021).
54. Fischer, G. et al. Global Agro-Ecological Zones (GAEZ v4) Model Documentation. FAO & IIASA, 303 pp (2021).
55. Schiavina, M. et al. GHS-POP ARCTIC R2025A – gridded population estimates for the Arctic region (1975-2030). European Commission, Joint Research Centre (2026).
56. Lizana, J. et al. Global gridded dataset of heating and cooling degree days under climate change scenarios. Nat. Sustain. 9, 470–480 (2026).
57. Tarnocai C. & Bockheim J. Cryosolic soils of Canada: Genesis, distribution, and classification. Can. J. Soil Sci. 91(5): 749-762 (2011).
58. Zhegusov, Y.I. & Maximov, T. Kh. Public Perception of Climate Change Impact on Living Conditions in a Cold Region (the case of the Republic of Sakha (Yakutia)). Sotsiologicheskie Issledovaniia 145 – 151 (2024).
59. Mishra, U. et al. Spatial heterogeneity and environmental predictors of permafrost region soil organic carbon stocks. Sci. Adv. 7, eaaz5236 (2021).
60. DeLuca T. H, et al. Diazotrophy in alluvial meadows of subarctic river systems. PLoS ONE 8, e77342 (2013).
61. Karjalainen, O. et al. High-resolution predictions of ground ice content for the Northern Hemisphere permafrost region. Earth System Science Data Discussions, 1–40 (2022).
62. Lodygin, E., Vasilevich, R., & Abakumov, E. The Molecular Composition of Peat Organic Matter and Prospects for Its Use in Agriculture. Agronomy 13, 2414 (2023).
63. Granina, N.I., Martynova, N.A., & Kiseleva, N.D. Spatio-temporal heterogeneity of soil cover in Baikal area and its impact on the development of agriculture in the region. IOP Conf. Ser.: Earth Environ. Sci. 368, 012017 (2019)
64. Kawakita S., Takahashi H., & Moriya K. Prediction and parameter uncertainty for winter wheat phenology models depend on model and parameterization method differences, Agr. Forest Meteorol. 290, 107998, (2020).
65. Zhang, Y. et al. Future reversal of warming-enhanced vegetation productivity in the Northern Hemisphere. Nat. Clim. Change

12, 581–586 (2022).

66. Wang, J. & Liu, D. Vegetation green-up date is more sensitive to permafrost degradation than climate change in spring across the northern permafrost region. Glob. Change Biol. 28, 1569–1582 (2022).
67. Mauclet, E. et al. Changing sub-Arctic tundra vegetation upon permafrost degradation: Impact on foliar mineral element cycling. Biogeosciences 19, 2333–2351 (2022).
68. Price, M. J. Seeing Green: Lifecycles of an Arctic Agricultural Frontier. Rural Sociol. 88, 941–971 (2023).
69. Gartler, S. et al. A transdisciplinary, comparative analysis reveals key risks from Arctic permafrost thaw. Commun. Earth Environ. 6, 21 (2025).
70. Ford, J. D., et al. The rapidly changing Arctic and its societal implications. Wires. Clim. Change, 12(6), e735 (2021).
71. Bouchard, M. Un défi environnemental complexe du XXIe siecle au Canada: I'identification et la compréhension de la réponse des environnements face aux changements climatiques globaux. Can. Geogr-Geogr Can. 45, 54–70 (2001).
72. Parfenova, E., Tchebakova, N., & Soja, A. Assessing landscape potential for human sustainability and 'attractiveness' across Asian Russia in a warmer 21st century. Environ. Res. Lett. 14, 065004, (2019).
73. Prakash, S. et al. Cryospheric changes and livelihood vulnerability in Lahaul Region of North-Western Himalaya, India. Sustain. Water Resour. Manag. 10, 194 (2024).
74. Bousfield, C. G., Morton, O. & Edwards, D. P. Climate change will exacerbate land conflict between agriculture and timber production. Nat. Clim. Change 14, 1071–1077 (2024).
75. Peplau, T. et al. Subarctic soil carbon losses after deforestation for agriculture depend on permafrost abundance. Glob. Change Biol. 28, 5227–5242 (2022).
76. Monfreda, C., Ramankutty, N. & Foley, J. A. Farming the planet: 2. Geographic distribution of crop areas, yields, physiological types, and net primary production in the year 2000. Global Biogeochem. Cy. 22, GB1022 (2008).
77. FAOSTAT, Value of Agricultural Production (FAO, 2024).
78. Portmann, F. T., Siebert, S. & Doell, P. MIRCA2000-Global monthly irrigated and rainfed crop areas around the year 2000: A new high-resolution data set for agricultural and hydrological modeling. Global Biogeochem. Cy. 24, GB1011 (2010).
79. Manning, M.R. The treatment of uncertainties in the fourth IPCC assessment report. Adv. Clim. Chang. Res. 2, 13–21 (2006).
80. Dyderski, M. K. et al. How much does climate change threaten European forest tree species distributions? Glob. Change Biol. 24, 1150–1163 (2018).
81. Karger, D.N. et al. Climatologies at high resolution for the earth's land surface areas. EnviDat. (2021).
82. Taylor, P. J. et al. Southern Africa's Great Escarpment as an amphitheater of climate-driven diversification and a buffer against future climate change in bats. Glob. Change Biol. 30, e17344. (2024).
83. Ashraf, U. et al. Aligning renewable energy expansion with climate-driven range shifts. Nat. Clim. Change 14, 242–246 (2024).
84. Reinecke, R. et al. Uncertainty in model estimates of global groundwater depth. Environ. Res. Lett. 19, 114066 (2024).
85. Phillips, S. J. et al. Opening the black box: An open-source release of Maxent. Ecography. 40(7), 887–893 (2017).
86. Liu, H. et al. Study on climate suitability for maize and technical implementation strategies under conservation tillage in Northeast China. Soil Till. Res. 249, 106473 (2025).
87. Li, X. et al. Mapping cropland suitability in China using optimized MaxEnt model. Field Crop Res. 302, 109064 (2023).
88. Zheng, Q. et al. The neglected role of abandoned cropland in supporting both food security and climate change mitigation. Nat. Commun. 14, 6083 (2023).
89. Akabane, T. K. et al. Weaker Atlantic overturning circulation increases the vulnerability of northern Amazon forests. Nat. Geosci. 17, 1284–1290 (2024).

90. Fleiss, S. et al. Implications of zero-deforestation palm oil for tropical grassy and dry forest biodiversity. Nat. Ecol. Evol. 7, 250–263 (2023).
91. Thonis, A., Stansfield, A. & Akcakaya, H. R. Unravelling the role of tropical cyclones in shaping present species distributions. Glob. Change Biol. 30, e17232 (2024).
92. Marshall, L. et al. Potential for climate change driven spatial mismatches between apple crops and their wild bee pollinators at a continental scale. Global Environ. Chang. 83, 102742 (2023).
93. Eulalio, K. D. et al. Epidemiological, clinical, and genomic landscape of coccidioidomycosis in northeastern Brazil. Nat. Commun. 15, 3190 (2024).
94. Li, W.-B. et al. Human activity and climate change accelerate the extinction risk to non-human primates in China. Glob. Change Biol. 30, e17114 (2024).
95. Kass, J. M. et al. ENMeval 2.0: Redesigned for customizable and reproducible modelling of species' niches and distributions. Methods Ecol. Evol. 12, 1602–1608 (2021).
96. Velasco, J. A. & Gonzalez-Salazar, C. Akaike information criterion should not be a "test" of geographical prediction accuracy in ecological niche modelling. Ecol. Inform. 51, 25–32 (2019).
97. Warren, D. L. & Seifert, S. N. Ecological niche modeling in Maxent: The importance of model complexity and the performance of model selection criteria. Ecol. Appl. 21, 335–342 (2011).
98. Gruber, S. Derivation and analysis of a high-resolution estimate of global permafrost zonation. Cryosphere, 6, 221–233 (2012).
99. Chen, Y. et al. Northern-high-latitude permafrost and terrestrial carbon response to twosolar geoengineering scenarios. Earth Syst. Dynam. 14, 55–79 (2023).
100. Liu, C., White, M. & Newell, G. Selecting thresholds for the prediction of species occurrence with presence-only data. J. Biogeogr. 40, 778–789 (2013).
101. R Core Team. R: A language and environment for statistical computing [Manual]. (2024).
102. MathWorks. MATLAB (Version R2022a) [Computer software]. The MathWorks, Inc. (2022).

Acknowledgements

We are grateful to Hui Ju, Yang Yang, and Renjie Hou for their valuable feedback on the conceptualization and formal analysis.

Funding statements

S.X. and C.X. disclose support for the research of this work from the National Key Research and Development Program of China (2022YFF0801903) and the Faculty of Geographical Sciences, Beijing Normal University (2022-GJTD-01).

Author contributions

S.X. and C.X. conceived the study and developed the research framework. S.X. designed the methodology, conducted the analyses, interpreted the results, and wrote and revised the manuscript. C.X. supervised the study and contributed to the interpretation of the results and manuscript revision. J.J., V.E.R., Z.Z., J.D., B.S., and T.Z. provided important comments and constructive suggestions that substantially improved the manuscript. All authors reviewed, discussed, and approved the final version of the manuscript.

Competing interests

The authors declare no competing interests.

Fig. 1 | Northward shift of crop climatic suitability zones (CCSZ) under the SSP5–8.5 scenario during 2071–2100.
Here, CCSZ refer to single and limited double cropping zones, excluding areas of double and multiple cropping. (a) and (b) show CCSZ combining seven representative crops in North America and Eurasia, respectively. The red line represents the northern boundary of simulated CCSZ during the baseline (1980–2010) period (northern boundary of Supplementary Figure 2b).Shading from beige to green indicates increasing agreement among the five GCMs (values from 1 to 5). (c) Latitudinal distribution of individual crop suitable areas, calculated as the average across GCMs. The gray shading shows the baseline (1980–2010) distribution of suitable areas by latitude; the black solid line indicates future suitable areas; and the green shading represents the area of AF (grid cells classified as unsuitable in the baseline but projected to become suitable in the future) across latitudes.

Fig. 2 | Permafrost region, CCSZ, and areas of coexistence under the SSP5–8.5 scenario for 2071–2100.
Shaded areas in light to dark blue represent permafrost zones of different continuity levels. Gray patches indicate CCSZ (single and limited double cropping zones, averaged across GCMs). Green hatching shows areas of spatial overlap between permafrost region and CCSZ. (a) Permafrost distribution during the baseline period (1980–2010); panels (b), (c), and (d) show the projected permafrost extents under the best-fit, minimum, and maximum cases, respectively. The best-fit case represents projections based on the simulation that most closely matches observations, while the minimum and maximum cases correspond to the fastest and slowest projected rates of permafrost thaw; (e) Overlap areas between permafrost and CCSZ under each cases. Blue bars correspond to different permafrost continuity levels, consistent with the blue categories shown on the maps.

Fig. 3 | Ground ice content within AF and their area latitudinal distribution under the SSP5–8.5 scenario for 2071–2100.
In panels (a) and (c), colored patches represent AF areas: teal indicates AF converted from non-permafrost zones, while other colors denote AF derived from former permafrost zones of varying ice content. Blue hatching marks AF areas where permafrost remains under the best-fit case. Panels (b) and (d) show the latitudinal distribution of AF area. Grey shading indicates the total AF extent; blue areas represent AF converted from former permafrost zones; remaining colors correspond to areas transformed from low, medium, and high-ice-content permafrost, consistent with the legend in the maps.

Fig. 4 | Comprehensive suitability map of AF under the SSP5–8.5 scenario during 2071–2100, incorporating the impacts of permafrost.
Panels (a) and (b) show North America and Eurasia, respectively. The vertical axis of the legend (labeled 1 to 6) represents the permafrost impact categories (Cat.1 to Cat.6), while the horizontal axis (labeled 1 to 7) indicates crop abundance, i.e., the number of crop suitable in each grid cell , resulting in a total of 42 AF sub-classes. A horizontal black line divides the permafrost impact into two broad classes, with Cat. 1–Cat. 3 indicating that permafrost does not fundamentally overturn crop suitability and that the land remains cultivable after soil leveling and grading. Cat. 4–6 suggest that negative impacts associated with permafrost tend to dominate, potentially constraining cultivation due to ground surface disturbances and, in some cases, leading to farmland abandonment.

Table 1 Extent of different suitability zones in 2071-2100, SSP5–8.5 scenario (combinations of crop abundance and permafrost impact classification). Values before brackets indicate suitability area calculated under the best-fit permafrost case, whereas bracketed ranges reflect suitability area under the minimum and maximum permafrost cases. Units: For each category (Cat.), two metrics are reported: area (10^4 km²) and the percentage of AF represented by each sub-class. Categories 1–6 follow the definitions in the Results section (An integrated permafrost-informed crop suitability map).

Permafrost impact classification		Abundance of crops						
		1	2	3	4	5	6	7
Cat. 1	10^4 km²	30.61 (31.03, 26.07)	27.05 (27.08, 24.95)	39.10 (39.10, 37.08)	68.58 (68.59, 67.01)	54.89 (54.89, 54.44)	39.14 (39.14, 39.04)	8.46 (8.46, 8.43)
	%	2.63 (2.67, 2.24)	2.32 (2.33, 2.14)	3.36 (3.36, 3.19)	5.89 (5.89, 5.76)	4.72 (4.72, 4.68)	3.36 (3.36, 3.35)	0.73 (0.73, 0.72)
Cat. 2	10^4 km²	113.24 (123.62, 37.28)	82.83 (87.09, 39.24)	106.28 (111.68, 59.53)	118.79 (124.02, 85.83)	79.06 (79.24, 65.19)	49.03 (49.04, 43.18)	24.12 (24.12, 21.96)
	%	9.73 (10.62, 3.20)	7.12 (7.48, 3.37)	9.13 (9.60, 5.12)	10.21 (10.66, 7.38)	6.79 (6.81, 5.60)	4.21 (4.21, 3.71)	2.07 (2.07, 1.89)
Cat. 3	10^4 km²	17.41 (17.98, 5.53)	17.48 (17.62, 8.56)	21.00 (21.04, 9.04)	30.11 (30.81, 24.00)	12.63 (12.65, 9.20)	7.50 (7.50, 6.67)	1.77 (1.77, 1.71)
	%	1.50 (1.54, 0.48)	1.50 (1.51, 0.74)	1.80 (1.81, 0.78)	2.59 (2.65, 2.06)	1.09 (1.09, 0.79)	0.64 (0.64, 0.57)	0.15 (0.15, 0.15)
Cat. 4	10^4 km²	47.48 (37.85, 149.71)	19.02 (14.36, 81.67)	19.47 (13.18, 91.36)	19.61 (13.30, 69.01)	0.26 (0.06, 19.73)	0 (0, 7.15)	0 (0, 2.35)
	%	4.08 (3.25, 12.87)	1.63 (1.23, 7.02)	1.67 (1.13, 7.85)	1.69 (1.14, 5.93)	0.02 (0, 1.70)	0 (0, 0.61)	0 (0, 0.20)
Cat. 5	10^4 km²	17.43 (20.31, 4.05)	16.74 (17.56, 8.18)	23.47 (24.31, 11.69)	23.14 (23.52, 14.37)	11.52 (11.52, 9.80)	9.04 (9.04, 8.68)	2.20 (2.20, 2.10)
	%	1.50 (1.75, 0.35)	1.44 (1.51, 0.70)	2.02 (2.09, 1.00)	1.99 (2.02, 1.24)	0.99 (0.99, 0.84)	0.78 (0.78, 0.75)	0.19 (0.19, 0.18)
Cat. 6	10^4 km²	4.64 (0.02, 8.16)	0.59 (0, 1.11)	0 (0, 0.62)	0 (0, 0)	0 (0, 0)	0 (0, 0)	0 (0, 0)
	%	0.40 (0, 0.70)	0.05 (0, 0.10)	0 (0, 0.05)	0 (0, 0)	0 (0, 0)	0 (0, 0)	0 (0, 0)

Editorial Summary:

Permafrost may limit the suitability of up to 29% of newly suitable agricultural land in high latitudes under global warming, according to simulations integrating permafrost degradation and crop suitability for seven major crops.

Peer review information:

Communications Earth and Environment thanks Andrew Spring, Norman Julius Steinert and the other, anonymous, reviewer(s) for their contribution to the peer review of this work. Primary Handling Editor: Nicola Colombo. A peer review file is available.

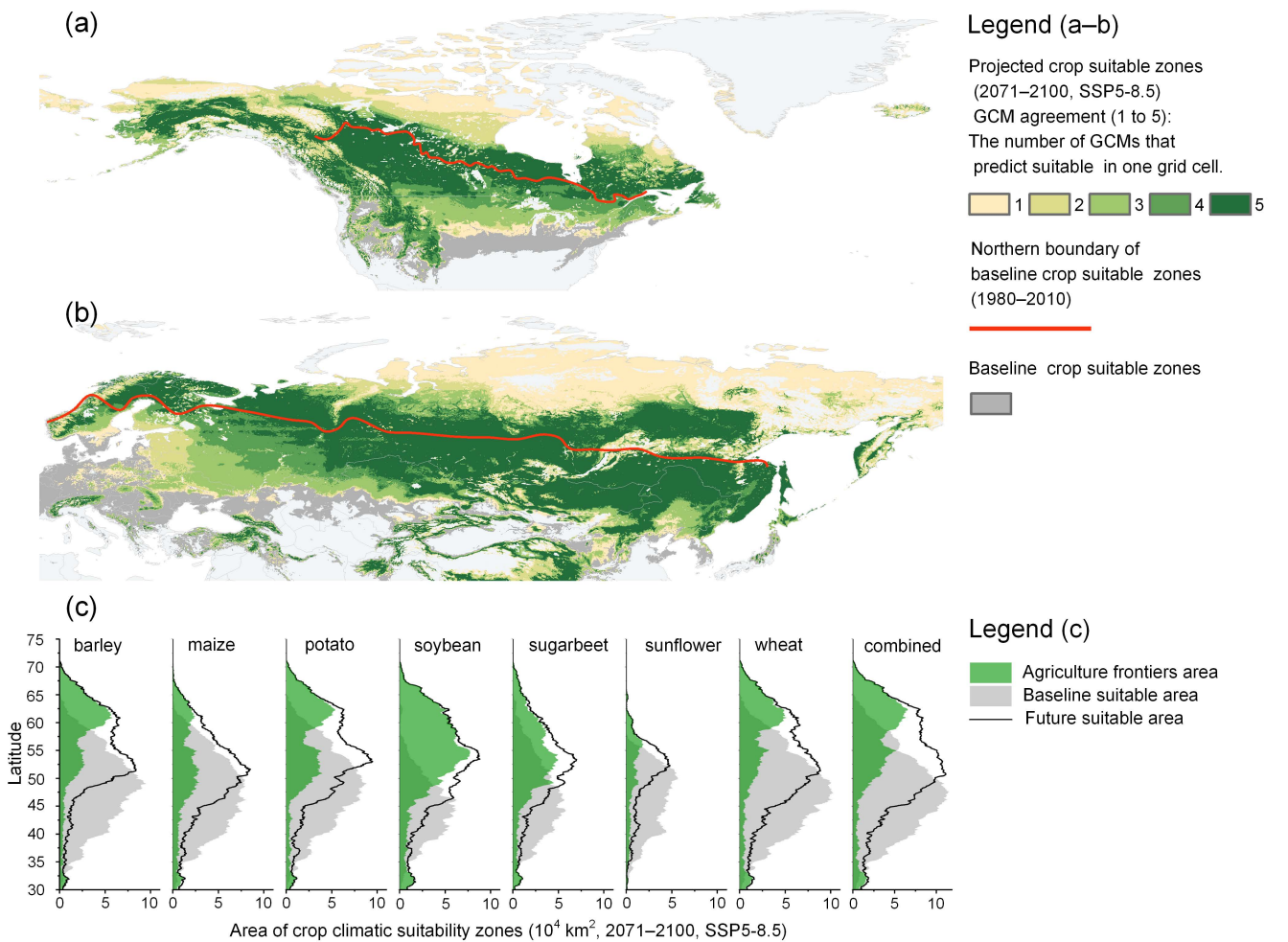
(a)
(b)
Legend (a–b)
Projected crop suitable zones
(2071–2100, SSP5-8.5)
GCM agreement (1 to 5):
The number of GCMs that
predict suitable in one grid cell.
1
2
3
4
5
Northern boundary of
baseline crop suitable zones
(1980–2010)
Baseline crop suitable zones
(c)
barley
maize
potato
soybean
sugarbeet
sunflower
wheat
combined
Latitude
75
70
65
60
55
50
45
40
35
30
0
5
10
Area of crop climatic suitability zones (10^4 km^2, 2071–2100, SSP5-8.5)
Legend (c)
Agriculture frontiers area
Baseline suitable area
Future suitable area

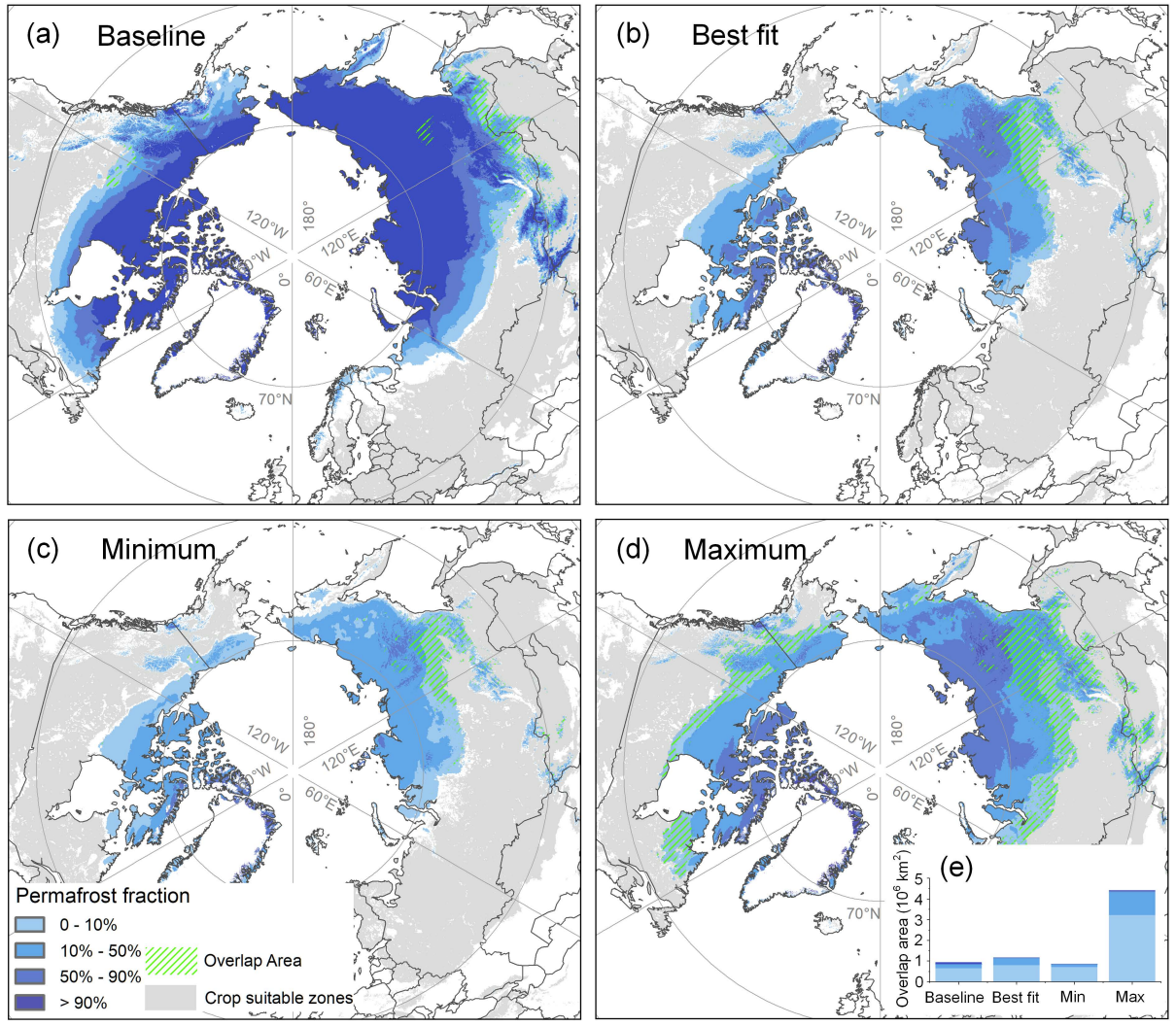
(a) Baseline
(b) Best fit
(c) Minimum
(d) Maximum
120°W
180°
120°E
60°W
0°
60°E
70°N
Permafrost fraction
0 - 10%
10% - 50%
50% - 90%
> 90%
Overlap Area
Crop suitable zones
(e)
Overlap area (10^6 km^2)
0
1
2
3
4
5
Baseline
Best fit
Min
Max

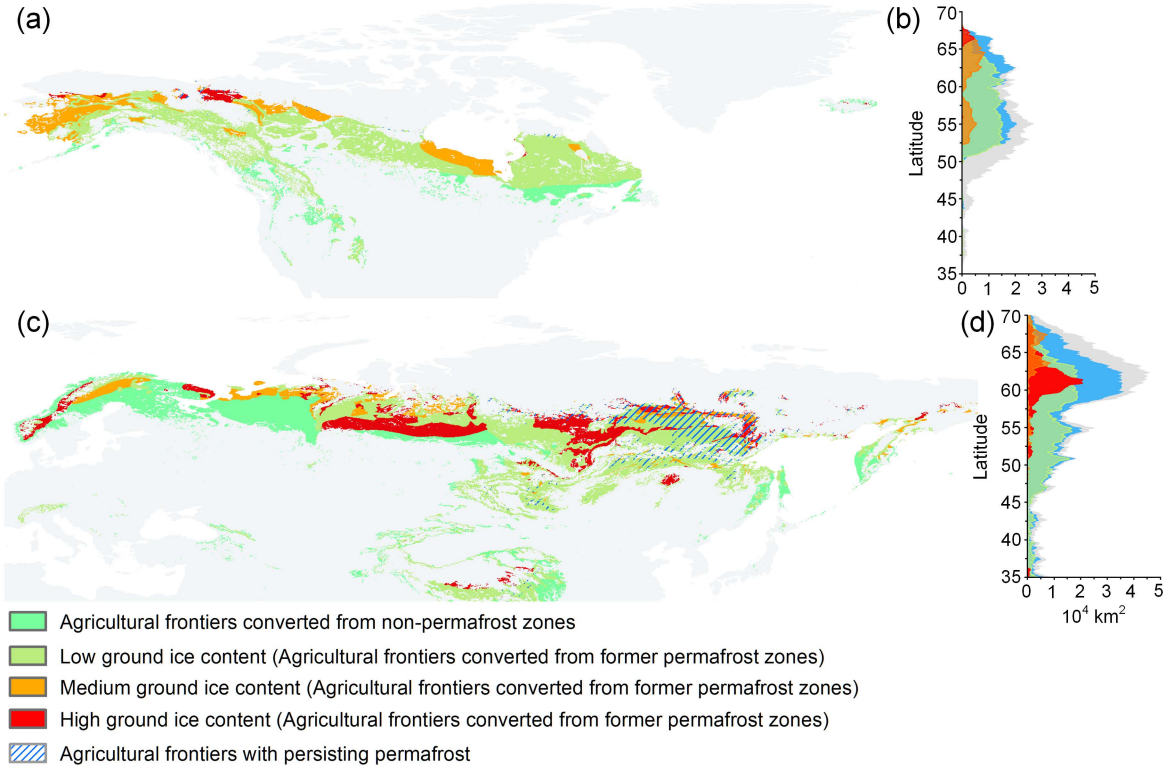
(a)
(b)
(c)
(d)
Latitude
70
65
60
55
50
45
40
35
0 1 2 3 4 5
10^4 km^2
Agricultural frontiers converted from non-permafrost zones
Low ground ice content (Agricultural frontiers converted from former permafrost zones)
Medium ground ice content (Agricultural frontiers converted from former permafrost zones)
High ground ice content (Agricultural frontiers converted from former permafrost zones)
Agricultural frontiers with persisting permafrost

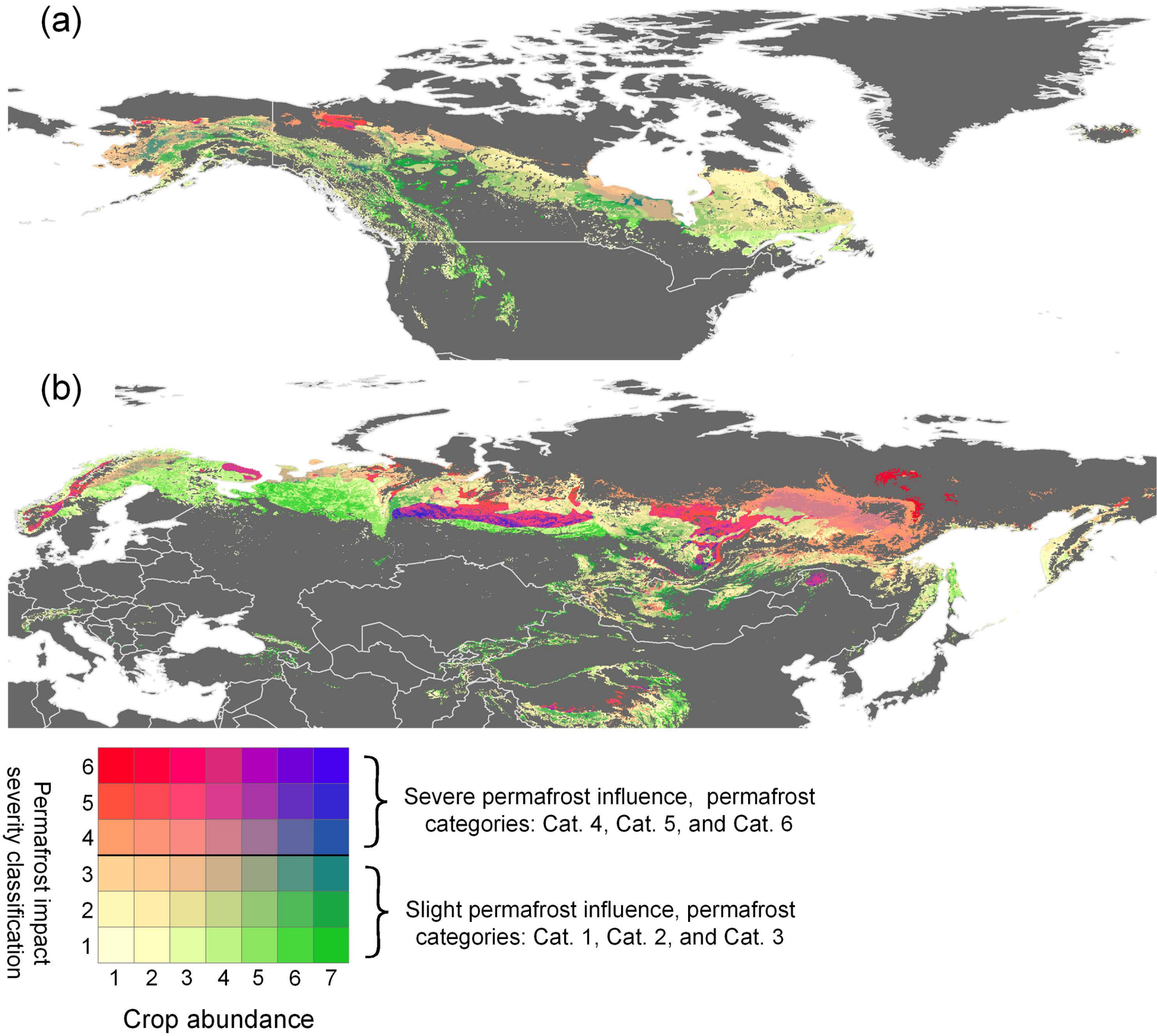
(a)
(b)
6
5
4
3
2
1
Permafrost impact severity classification
1 2 3 4 5 6 7
Crop abundance
Severe permafrost influence, permafrost categories: Cat. 4, Cat. 5, and Cat. 6
Slight permafrost influence, permafrost categories: Cat. 1, Cat. 2, and Cat. 3